Available online at www.sciencedirect.com

ScienceDirect

Energy Procedia 1 (2009) 3091–3098

Energy Procedia

www.elsevier.com/locate/procedia

GHGT-9

CO_2 injectivity into brine aquifers: why relative permeability matters as much as absolute permeability

McMillan Burton, Navanit Kumar and Steven L. Bryant*

The University of Texas at Austin, 1 University Station C0304, Austin, TX 78712, USA

Abstract

For economic reasons operators of geologic storage projects are likely to inject CO_2 at the largest possible rates into the smallest number of wells. Thus a typical CO_2 injection well is likely to run at the largest bottomhole pressure that is safe. Operators will also tend to prefer thicker, higher permeability target formations. However, a constant-pressure well exhibits a varying rate of CO_2 injection for two reasons: classical multiphase flow effects, and long-term injection of CO_2 removes water from the near-wellbore region. Drying precipitates dissolved salts, so the permeability of the dry rock need not equal the initial aquifer permeability. Mobility of CO_2 in the dried rock and mobility of CO_2 and brine the two-phase flow region determine the variation of injectivity with volume of CO_2 injected.

We find a four-fold variation in injectivity when seven different CO_2/brine relative permeability curves (Bennion and Bachu [1]) are used, holding all other reservoir parameters the same. Since the product of formation permeability and formation thickness is relatively easy to measure, once a well has been drilled, uncertainty in relative permeability will therefore be a large contribution to uncertainty in achievable rates in CO_2 storage projects.

We develop analytical expressions for the injectivity variation in terms of phase mobilities and the speeds of saturation fronts. Classical theory (Buckley-Leverett) does not account for the drying front; using only Buckley-Leverett yields both quantitative and qualitative errors. The expressions are consistent with detailed reservoir simulations using commercial software (CMG's GEM) that account for the full physics and complete phase behavior. The expressions can refine the estimated number of wells needed for a target overall injection rate. This analysis also enables an operator to assess the value of retrieving core and measuring relative permeability in a prospective storage target.

Keywords: Injectivity; geologic storage; relative permeability; fractional flow; well count

* Corresponding author. Tel.: 512-471-3250; fax: 512-471-9605.
E-mail address: steven_bryant@mail.utexas.edu.

doi:10.1016/j.egypro.2009.02.089

1. Introduction

Geologic sequestration of CO_2 can mitigate the effect of increasing CO_2 emission these emissions, but very large injection rates will be needed. For example, injecting 1 Gt C per year at typical deep saline aquifer conditions would correspond to a reservoir conditions flow rate similar to the current global production of oil (over 80 million barrels per day). Thus, high injectivity will be essential to reduce the cost of geologic sequestration at this scale.

The first order effect on injectivity is the product of formation permeability and formation thickness, *kh.* Subsurface formations with large *kh* are the preferred targets for storage. The main message of this paper is that all else is not equal, and *kh* should not be the only criterion for site selection. Mutual solubility (of CO_2 in the aqueous phase and H_2O in the CO_2-rich phase) and the relative permeabilities to brine and CO_2 can alter injectivity by a factor of four in the formations examined here. Moreover, the injectivity will vary with volume injected.

Three regions of flow are identified that will develop in the aquifer. The regions are (1) dry CO2 in the near-wellbore region; (2) the Buckley-Leverett or two-phase region, and (3) the brine region far from the well. As shown in Figure 1, the three regions are separated by two fronts that move at characteristic speeds (Noh et al. [2]). Because of mutual solubility, the situation differs from classical two-phase immiscible flow, which has a single front separating two regions.

We develop a simple 1D model of injection at constant pressure using Darcy's Law and a modified form of Buckley-Leverett fractional flow theory, which accounts for partial solubility of CO_2 and H_2O in each phase. The front speeds and region mobilities can be evaluated directly from the inputs of phase behavior, relative permeability curves, and viscosities. We use this model to evaluate sensitivities to features of the relative permeability curves (endpoints, curvature, etc.); phase behavior (temperature and pressure dependence of solubility); and salt precipitation due to drying. We apply the model to a sandstone formation in Alberta, and then evaluate the effect of the relative permeability on injectivity using laboratory measurements on several formations in the Alberta Basin reported by Bennion and Bachu [1]. The data are for CO_2 and brine (both saturated) in sandstones and carbonates from several aquifers. The curves differ significantly between samples.

As the drying front moves deeper into the formation, large saturations of brine will be evaporated precipitating all remaining salt which will in turn decrease the permeability to the dry gas phase. We examine the impact of this effect and a method to measure it in the laboratory.

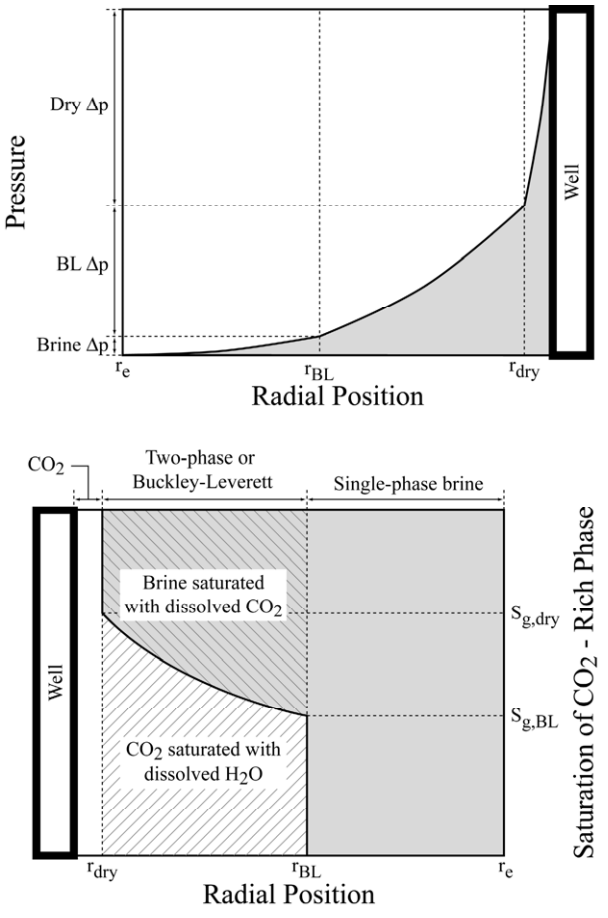

Fig. 1—Three regions of flow develop during CO_2 injection into an aquifer. (TOP) Pressure gradient decreases with radius, but rate of decrease differs in each region because phase mobilities vary. (BOTTOM) Fractional flow curve modified to account for CO_2 /H_2O phase behavior (Noh *et al*. [2]) determines the position of the fronts and the saturations in the two-phase Buckley-Leverett region.

2. 2. Modeling Approach

2.1. Overview and assumptions

We use a simplified one dimensional reservoir model, Figure 1, extending to a drainage radius of r_e = 10,000 ft. It has homogeneous properties. We assume constant pressure boundaries at the wellbore and the drainage radius. The injection rate, q, will vary with time. We assume that the pressure gradients can be computed from the flow rate at any instant as though the flow were at steady state. We further assume that fractional flow theory can be applied to this situation of

variable flow rate. Compressibility is ignored, and viscosities of each phase are assumed constant and independent of composition. Wherever the CO_2-rich and aqueous phases are in contact, we assume they are in chemical equilibrium. Temperature is assumed constant, and no geochemical reactions occur. Precipitation of the dissolved solids is considered after the basic theory is developed.

2.2. Phase Mobility and Relative Permeability Curves.

The mobility of a phase *j* is given by $M_j = k_{rj} / \mu_j$ where k_r is relative permeability and μ is viscosity. The fractional flow of phase *j* is given by

$$f_j = \frac{M_j}{M_j + M_i} \tag{1}$$

where *i* denotes the other phase.

Bennion and Bachu [1] measured relative permeability curves on seven cores from deep formations in western Canada. The experiments were performed with CO_2-saturated brine and brine-saturated CO_2 to insure that drying fronts did not affect the measurements. We fit their reported data to the following Corey-type equations:

$$k_{rw} = \left[1 - \left(\frac{S_g}{1 - S_{wr}}\right)\right]^m \qquad k_{rg} = k_{rg}^o \left[\frac{S_g}{1 - S_{wr}}\right]^n \tag{2}$$

where *w* and *g* indicate aqueous and CO_2-rich phases, respectively.

2.3. Relationship Between Pressure Drop and Flow Rate

Three regions of flow arise when CO_2 is injected into an aquifer, Figure 1. Farthest upstream (closest to injection well) is single-phase dry CO_2 flowing in dry rock. The drying front separates this region from the two-phase region, where the phase saturations vary continuously with position. The Buckley-Leverett front separates the two-phase region from the single-phase brine.

2.4. CO_2 Region

The total pressure drop will be the sum of the pressure drops across the three regions defined earlier. The pressure drop across the single-phase CO_2 region is estimated from the steady-state radial flow equation:

$$\Delta p_{dry} = \frac{q \mu_{CO_2}}{2\pi k h k_{r,S_g=1}} \ln\left(\frac{r_{dry}}{r_w}\right) \tag{3}$$

where $k_{r,S_g=1} = k_{salt}/k_{abs}$ is the permeability reduction due to salt precipitation. A simple estimate of this parameter is discussed by Burton et al 2008. Recall that the flow rate *q* is a function of time and the injection pressure is fixed.

2.5. Two-phase Region.

The pressure drop across the two-phase Buckley-Leverett region can be approximated by:

$$\Delta p_{BL} = \frac{q}{2\pi k h}\left(k_{rg}/\mu_g + k_{rw}/\mu_w\right)^{-1}\Big|_{S_{g,avg}} \ln\left(\frac{r_{BL}}{r_{dry}}\right) \tag{4}$$

The approximation replaces the radial-position-weighted mobility with the mobility at some average saturation within the two-phase region. This is reasonable if the range of saturations in the two-phase region is not too broad. This applied to the measured relative permeability curves used here. We take $S_{g,avg} = (S_{g,dry} + S_{g,BL})/2$ as a convenient estimate, where $S_{g,dry}$ is the CO_2 phase saturation in the two-phase region just downstream of the drying front, and $S_{g,BL}$ is the CO_2 phase saturation in the two-phase region just upstream of the Buckley-Leverett front.

2.6. Brine Region

The pressure drop across the single-phase brine region is:

$$\Delta p_{Brine} = \frac{q\mu_w}{2\pi kh}\ln\left(\frac{r_e}{r_{BL}}\right) \tag{5}$$

The total pressure drop across the reservoir yields the following:

$$\Delta p = \Delta p_{dry} + \Delta p_{BL} + \Delta p_{BRINE} = \frac{q}{2\pi kh}\left[\frac{\mu_g}{k_{r,Sg=1}}\ln\left(\frac{r_{dry}}{r_{sf}}\right) + \left(\frac{k_{rg}}{\mu_g} + \frac{k_{rw}}{\mu_w}\right)^{-1}\Bigg|_{S_{g,avg}} \ln\left(\frac{r_{BL}}{r_{dry}}\right) + \mu_w \ln\left(\frac{r_e}{r_{BL}}\right)\right] \tag{6}$$

Because the total pressure drop is prescribed, our goal is to find the instantaneous flow rate q. This is easily accomplished if the positions of the fronts r_{dry} and r_{BL} are known. The frontal positions are determined in the next section from the dimensionless cumulative injected volume (t_D) and the fractional flow curves. Thus Eq. 6 is an implicit equation for q.

3. Modified Buckley-Leverett Theory

The speed of the fronts and the phase saturations on either side of the fronts can be determined by using the fractional flow curve, constructing tangents to that curve which account for conservation of mass of CO_2 in the fluid phases (Noh *et al*. [2]). We summarize the application to radial flow elaborated by Burton et al. [3]. Buckley-Leverett theory for radial flow states:

$$\frac{r_D^2\big|_{Sg}}{t_D} = \left.\frac{df_g}{dS_g}\right|_{Sg} \tag{7}$$

Equation 7 can be applied to the saturation just downstream of the drying front, $S_{g,dry}$ as well as to the saturation just upstream of the two-phase flow front, $S_{g,BL}$, Figure 1. The dimensionless cumulative injected volume, t_D, is given by:

$$t_D = \int_o^t \frac{q(t)}{\pi r_e^2 h\phi}dt \tag{8}$$

The dimensionless radial position, r_D, is defined as $r_D = r/r_e$. The dimensionless velocity of the drying front and Buckley-Leverett front as defined by Noh *et al*. [2] are:

$$v_{D,dry} = \left.\frac{df_g}{dS_g}\right|_{S_{g,dry}} = \frac{f_{g,dry} - D_{BL\to dry}}{S_{g,dry} - D_{BL\to dry}} \qquad v_{D,BL} = \left.\frac{df_g}{dS_g}\right|_{S_{g,BL}} = \frac{f_{g,BL} - D_{brine\to BL}}{S_{g,BL} - D_{brine\to BL}} \tag{9}$$

Analogously to $S_{g,dry}$ and $S_{g,BL}$, $f_{g,dry}$ is the fractional flow just upstream of the drying front, and $f_{g,BL}$ is the fractional flow just downstream of the Buckley-Leverett front. $D_{BL\to dry}$ and $D_{brine\to BL}$ are defined by the phase concentrations in the different regions (Noh *et al*. [2]). $D_{BL\to dry}$ and $D_{brine\to BL}$ are therefore functions of temperature, pressure, and salinity. For the purposes of computing phase concentrations the pressure in the dry region was assumed to be the bottomhole injection pressure. The pressure in the Buckley-Leverett region was assumed to be 200 psi above the drainage radius pressure. Changes to pressure, temperature, and salinity have only a relatively small influence on injectivity. The speed of the fronts will remain constant with time and volume injected. Consequently their ratio, v_{BL}/v_{dry}, is also constant.

The radial positions needed for Eq. 6 are related to cumulative volume injected (i.e. dimensionless time) and the frontal speeds:

$$r_{dry} = r_e\sqrt{t_D v_{D,dry}} \qquad r_{BL} = r_e\sqrt{t_D v_{D,BL}} \tag{10}$$

The ratio of the drying front position and the Buckley-Leverett position, r_{BL}/r_{dry}, is also independent of the time. This fact will simplify the evaluation of effective mobility below.

$$r_{BL}/r_{dry} = \sqrt{v_{D,BL}/v_{D,dry}}$$

3.1. Effective Mobility

The effective mobility of fluid in this reservoir, M_{eff}, is the term in brackets on the right-hand side of Eq. 6. We rewrite it as the harmonic average of fluid mobility in each of the three regions:

$$\frac{\ln\left(\frac{r_e}{r_w}\right)}{M_{eff}} = \frac{\ln\left(\frac{r_e}{r_{BL}}\right)}{M_{brine}} + \frac{\ln\left(\frac{r_{BL}}{r_{dry}}\right)}{M_{BL}} + \frac{\ln\left(\frac{r_{dry}}{r_w}\right)}{M_{dry}} \tag{11}$$

Here we have introduced the following definitions:

$$M_{BL} = \left(k_{rg}/\mu_g + k_{rw}/\mu_w\right)\Big|_{S_{g,avg}} \qquad M_{brine} = \frac{1}{\mu_w} \qquad M_{dry} = \frac{k_{r,Sg=1}}{\mu_g}$$

On simplification

$$1/M_{eff} = C_1 + C_2 \ln\left(r_{dry}\right)\left(1/M_{dry} - 1/M_{brine}\right) \tag{12}$$

where C_1 and C_2 are positive constants. The effective mobility varies with time simply because the drying front advances into the reservoir with time. For typical deep saline aquifers, M_{brine} is likely to be less than M_{dry} because the viscosity of the CO_2-rich phase is usually much less than the viscosity of the brine. When M_{brine} is less than M_{dry}, the denominator of Eq. 12 decreases and M_{eff} increases as r_{dry} increases.

3.2. Application of Reservoir Simulation Software

To verify the above development, we applied the GEM simulator (Nghiem *et al*. [4]) to a cylindrical grid with 500 radial grid blocks. An injection well in the center block and a constant pressure production well in the outermost block allowed us to impose a fixed Dp across the domain. The simulator models the phase behavior using a Peng-Robinson equation-of-state, tuned by Kumar *et al*. [5] to fit $CO_2/H_2O/NaCl$ solubility data. The relative permeability lookup table must be modified to handle the value of $k_{r,Sg=1}$ upstream of the drying front.

4. Results and Discussion

We use the Viking sandstone of Alberta, Canada, to demonstrate the implementation of the modified Buckley-Leverett theory. Then we discuss the role of mobility in each of region. Finally, we show the sensitivity of the flow rate to relative permeability.

4.1. Field Example

The reservoir properties are summarized in Table 1. The relative permeability for the Viking sandstone reported by Bennion and Bachu [1] is shown in Figure 2(a). Using these data and the

Table 1—Viking Sandstone Properties

Property	*Value*	*Unit*
Permeability	30	md
Height	100	ft
Depth	4100	ft
Temperature	91	°F
Initial Pressure	1800 [a]	psi
Bottomhole Pres.	2800	psi
Salinity	30,000	ppm
Gas Visc., μ_{gas}	0.17	cp
Brine Visc., μ_w	0.7	cp
Porosity, ϕ	13.5	%
Edge radius, r_e	10,000	ft
$D_{BL\rightarrow Brine}$	1.0469 [b]	
$D_{dry\rightarrow BL}$	-0.0582 [b]	

[a] Hydrostatic pressure at depth.
[b] 2800 psia for dry CO_2 region and 2000 psia was used for brine and Buckley-Leverett region in the calculations of the "D" parameters

viscosities of the aqueous and CO_2 phases, the fractional flow curves can be constructed (see Figure 2(b)).

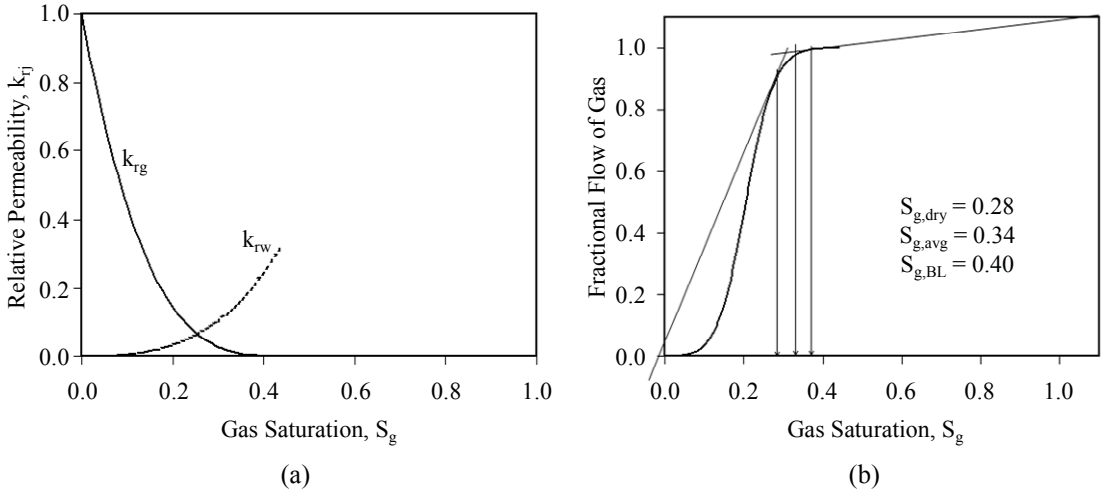

Fig. 2—(a) The relative permeability curves for the Viking Sandstone were measured by Bennion and Bachu [1]. (b) The fractional flow curve for the Viking Sandstone constructed from the relative permeabilities. Significant CO_2 saturations are shown with arrows and as values. The gas saturations occurring in the two-phase region of the reservoir will be between 0.28 and 0.40. The average gas saturation, Sg,avg = 0.34, is used to simplify the calculation of effective mobility.

Using the equations derived above and the properties in Table 1, we compute the injection rate for the reservoir and pressure drop across each region as a function of time. A constant pressure drop of 1,000 psi is applied to the reservoir for the 10,000 days of injection. Eq. 6 is solved at each time step by varying the flow rate using a spreadsheet solver until convergence is reached. The process is then repeated for each additional time step. In Figure 3, the flow rate is shown for our theory and from a GEM simulation of the same system. The curves differ by only 2%.

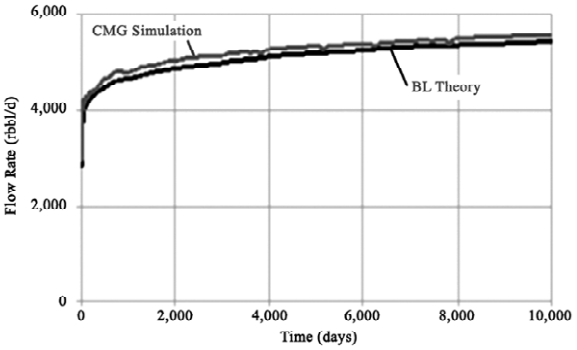

Fig. 3—During 10,000 days of injection of CO_2 at a constant 1,000psi pressure differential, the injection rate increases steadily. The rate determined from our simplified theory compares well with a full-fledged reservoir simulation for the same system.

Most importantly, the major trend is certainly captured by the simple theory. The injectivity increases steadily with time.

If mutual solubility between the CO_2 and brine were neglected, there would be no drying front. Injectivity would depend on the pressure drops in the single-phase brine region and the two-phase flow region. For the relative permeability curves of the Viking sandstone, the injection rate in this case would decrease with time, the opposite of the trend when the drying front occurs. Thus models or simulations that neglect H_2O solubility in CO_2 will overestimate the number of wells required for aquifer storage.

4.2. Mobility

The mobility in the Buckley-Leverett region has a significant effect on injectivity. But the nature of the effect is not obvious from comparing several relative permeability curves with different curvatures, endpoint permeabilities, and irreducible saturations. The evaluation techniques presented above permit direct comparison via mobility. The higher the average mobility in the Buckley-Leverett region (Eq. 11), the higher the flow rate, all else being equal. Simulations (Figure 4(a)) for seven different relative permeability curves confirm this (mobilities in Figure 4(b)). The seven relative permeability curves were measured by Bennion and Bachu [1]. Constant pressure injection was

simulated using the reservoir description of Table 1, substituting only the relevant lookup table for relative permeabilities in the input file.

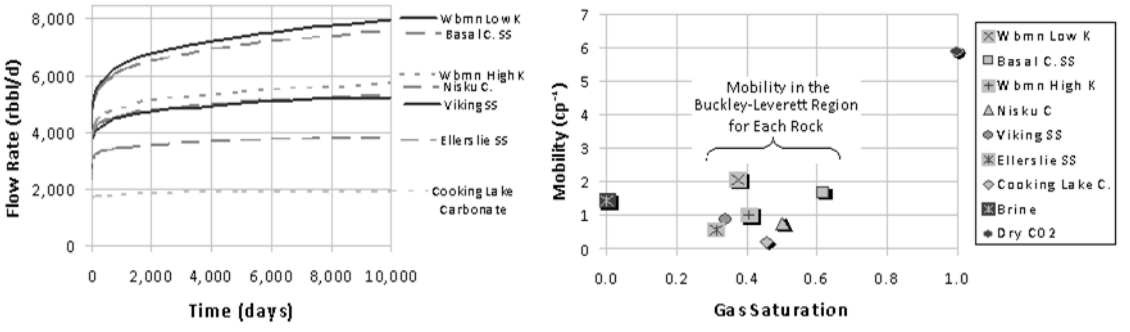

(a) (b)

Fig. 4—(a) Seven different relative permeability curves were published by Bennion and Bachu [1]. Each of those curves was used in conjunction with the formation properties in Table 1 to obtain this plot. Different mobility in the Buckley-Leverett region are responsible for the differences in injection rate. (b)—The mobility in the Buckley-Leverett region, evaluated at the average saturation, Sg,avg, is responsible for the differences in injection rate.The legend shows the formations in order of decreasing mobility in the Buckley-Leverett regions. The order is exactly the same as the arrangement of decreasing injection rate in (a).

The injection rate using the "Cooking Lake carbonate" relative permeability curves is four times smaller than the rate using the "Wabamun low permeability" curves. Of course the absolute permeabilities and thicknesses also vary between these formations, so the variation in injection rate would not be the same as depicted in Figure 4(a). The message here is the injectivity estimated only from the *kh* products for these formations would be wrong by a significant factor. The wide range of injection rates obtained in this study indicates that measuring relative permeability in the target formation is an important concern.

4.3. Sensitivity of Injectivity to Shape of Relative Permeability Curves

It is also instructive to examine the influence of the shape of the relative permeability curve on injectivity. Each Brooks-Corey fitting parameter for the Viking sandstone curves was varied (i.e. m, n, k^o_{rg}, S_{wr} from Eqs. 2). Figure 5 shows the resulting variation in injection rate (injection pressure being prescribed). The endpoint CO_2 relative permeability and the curvature of the aqueous phase relative permeability curve can change the injection rate by 20%. Therefore, uncertainty in relative permeability leads to uncertainty in flow rate and well count.

Recall that the $S_{g,avg}$ used in Eqs. 6 is an approximation of the mobility of the Buckley-Leverett region. Thus it is of interest to examine the sensitivity to $S_{g,avg}$. A perturbation of ±0.02 to $S_{g,avg}$ results in a ±10% change in flow rate.

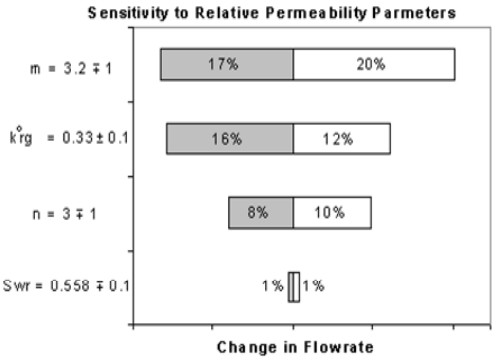

Fig. 5—We varied the parameters for the relative permeability equations (Eqs. 2) by the amounts shown. The flow rate varies by as much as 20% from changes in one parameter. Small uncertainties in the relative permeability curve can lead to important uncertainties in the flow rate.

5. Conclusion

Using Darcy's Law and Buckley-Leverett theory coupled to interphase mass transfer (mutual solubility), we developed a simple model for injectivity of CO_2 into an aquifer. Because CO_2 and H_2O are soluble in the aqueous and CO_2-rich phases, respectively, a drying front occurs, and the construction of classical Buckley-Leverett front is slightly modified. The two fronts move at constant speeds. Consequently, injectivity varies monotonically with volume injected. The two fronts define three regions of flow.

We show how to estimate the phase mobilities in each region from the relative permeability curves and the equation of state for the CO_2/brine system. In most formations, the mobility of CO_2 in the dry region exceeds the mobility of brine in the single-phase brine region. Thus injectivity will increase steadily. The trends of this simplified model agree well with simulations with full phase behavior. Neglecting the drying front underestimates the injectivity significantly; in most cases it predicts a monotonic decrease in injectivity. Hence accounting for compositional effects and fraction flow effects simultaneously is crucial to estimating injectivity .

Realistic variation in relative permeability curves (measured on seven formations in the Alberta Basin) yielded large variation in injectivity (a factor of four). Plausible changes in the parameters commonly used to characterize relative permeability curves yielded injectivity variation of up to 20%.

We conclude that quantifying the relative permeability curve is very important in determining achievable injection rate and therefore the well count for CO_2 geologic sequestration projects.

Acknowledgement

The authors are grateful to the sponsors of the Geologic CO_2 Storage Research Project at The University of Texas at Austin: BP, Chevron, CMG, ConocoPhillips, ExxonMobil, Landmark Graphics, Luminant and Shell.

References

1. Bennion, B. and Bachu, S., 2005. Relative permeability characteristics for supercritical CO_2 displacing water in a variety of potential sequestration zones in the western Canada sedimentary basin, Paper SPE 95547 at SPE Annual Technical Conference an Exhibition, Dallas, TX, 9-12 October.
2. Noh, M. Lake, L., Bryant, and Araque-Martinez, A. 2007. Implications of coupling fractional flow and geochemistry for CO_2 injection in aquifers, *SPEREE* **10** (4): 406-411. SPE 89341-PA.
3. Burton, M., Kumar, N. and Bryant, S. Time-Dependent Injectivity During CO_2 Storage in Aquifers. SPE 113937 presented at 2008 SPE Improved Oil Recovery Symposium held in Tulsa, Oklahoma, U.S.A., 19–23 April 2008
4. Nghiem, L., Sammon, P., Grabenstetter, J., and Ohkuma, H. 2006. Modeling CO_2 storage in aquifers with a fully-coupled geochemical EOS compositional simulator. Paper SPE 89474 presented at 2006 SPE/DOE Symposium on Improved Oil Recovery, Tulsa, Oklahoma, 22-26 April.
5. Kumar, A., Noh, M., Pope, G., Sepehrnoori, K., Bryant, S., and Lake, L. 2005. Reservoir simulation of CO_2 storage in deep saline aquifer, *SPEJ* **10** (3): 336-348. SPE 89343-PA.